A NEW IMPACT PICTURE FOR LOW AND HIGH ENERGY PROTON-PROTON ELASTIC SCATTERING *

C. BOURRELY and J. SOFFER
Centre de Physique Théorique, CNRS, MARSEILLE +
and
Tai Tsun WU ++
Instituut voor Theoretische Fysica, Rijksuniversiteit, Utrecht

ABSTRACT : We improve significantly the impact picture that was used several years ago to predict the increase of total and integrated differential cross sections at high energies. The major improvements consist of the following : (1) the dependence of the Pomeron term on the momentum transfer is taken from a modified version of the relation between matter distribution and charge distribution ; (2) Regge backgrounds are properly taken into account ; and (3) a simple non-trivial form is used for the hadronic matter current in the proton. For proton-proton elastic scattering, the phenomenological differential cross section is in good agreement with the experimental data in the laboratory momentum range of 14 GeV/c to 2000 GeV/c, and is predicted for ISABELLE energy. Because of the third improvement, predictions are obtained for both polarization and R parameters for proton-proton elastic scattering.

78/P.992

MAY 1978

++ On leave from Harvard University, Cambridge, Massachusetts 02138.
* Work supported in part by U.S. Department of Energy contract n° EY-76-S-02-3227

+ Postal Address : Centre de Physique Théorique - CNRS
31, chemin Joseph Aiguier
F - 13274 MARSEILLE CEDEX 2 (France)

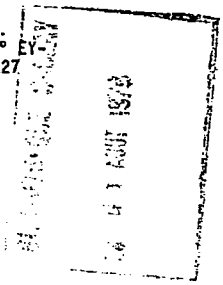

I - INTRODUCTION

In order to have some theoretical understanding of scattering processes at extremely high energies, one useful approach is to study the high-energy behavior of quantum field theory. In any relativistic quantum field theory, many fundamental properties of the S-matrix are automatically satisfied, including in particular the presence of production processes, s-channel unitarity, t-channel unitarity, analyticity, and crossing symmetry. For this reason, in relativistic quantum field theory we have a theoretical laboratory to investigate the interrelation of these general properties together with their implications on high-energy processes.

A first result of such an investigation [1] is that the Froissart bound [2] is not merely an upper bound but is actually saturated. In other words, in the high energy limit $s \to \infty$, the total cross section increases as $(\ln s)^2$, where s is the square of the center-of-mass energy. Three years later, this prediction of increasing cross section was experimentally verified at ISR for proton-proton scattering [3]. By now, there is a great deal of experimental information on this subject from both ISR and Fermilab. It is the purpose of this paper to carry out a phenomenological analysis of these data on proton-proton scattering in a way compatible with the results of quantum field theory.

Several years ago, when there was as yet very little experimental information, such a phenomenological analysis, referred to as an impact picture, was carried out [4]. This earlier analysis was successful in giving a number of predictions that were verified later, such as the increase of the πp and Kp total cross sections, and the large ratio of Kp to pp differential cross sections. However, this earlier analysis (see for a more recent summary [5]) also has a number of major defects ; the present work contains the following significant improvements :

(i) In the dependence on momentum transfer, the form of the Pomeron term is taken from a modified version of the relation between matter distribution and charge distribution [6 , 7]. In the earlier analysis [4], because of the absence of data, this form was chosen arbitrarily for computational convenience.

(ii) In the dependence on energy, Regge background terms are properly included. In the earlier analysis, these terms are taken into account only in the forward direction.

(iii) The spin dependence of the proton in the Pomeron term is constructed within a simple physical picture of rotation of matter inside the proton. This construction is based on the concept of hadronic current density of Chou and Yang [8]. It is thus possible to study the polarization and rotation parameters.

On the other hand, a number of the simplifying assumptions used previously [4] are still retained. They include in particular the following two :

(1) The contribution to opaqueness due to the Pomeron is assumed to be factorized into the product of a function of energy and one of the impact parameter [see (2) below]. This factorization is sometimes referred to as geometrical scaling.

(2) The opaqueness for any fixed impact parameter is assumed to increase without bound in the limit of infinite energy.
It must be realized that neither of these assumptions has support from quantum field theory [1] , and almost certainly requires modification in the future. In particular, the second assumption means that we use the factor $1 - e^{-\Omega(s,\vec{b})}$ below in (1) while it should more generally be $\propto \left[1 - e^{-\Omega(s,\vec{b})}\right]$ with $\propto \leq 1$. This assumption has been extensively discussed before [see Sec. 4(H) of reference 4], and the presence of $\propto < 1$ means, on the basis of quantum field theory, the most interesting possibility of the existence of hadronic states that couple very weakly to the Pomeron.

The present phenomenological analysis covers the range in laboratory momentum from 14 GeV/c to 2000 GeV/c. Special attention is given to the absence of the second dip in pp differential cross section. Predictions for energies of future accelerators such as ISABELLE are presented.

II - DESCRIPTION OF THE MODEL

In this section we describe our model in view of an analysis of the experimental data on total and differential cross sections. In the impact parameter representation we write the proton-proton elastic amplitude as

$$H(s,t) = \frac{is}{2\pi} \int e^{-i\vec{q}\vec{b}} \left(1 - e^{-\Omega(s,\vec{b})}\right) d\vec{b} \qquad (1)$$

where $\vec{q}$ is the momentum transfer, $t = -\vec{q}^2$ and $\Omega(s,\vec{b})$ is defined to be the opaqueness at the impact parameter $\vec{b}$ which is also a function of the energy $\sqrt{s}$. The colliding particles carry a spin one-half and as a result $\Omega(s,\vec{b})$ is a spin dependent function. The spin dependence of Ω will be treated in section IV and for the moment let us define $\Omega_0(s,\vec{b})$ corresponding to the spin independent part of the amplitude as a sum of two terms

$$\Omega_0(s,\vec{b}) = S_0(s) F(\vec{b}^2) + R_0(s,\vec{b}) \qquad (2)$$

the first term associated to the "Pomeron" exchange is responsible for the diffractive component and the second term is a Regge background whose contribution is needed to describe the low energy data. For the diffrac-

tive term a simple choice is to assume [4] that the s and the $\vec{b}$ dependence factorize such that we have a product of two function $S_o(s)$ and $F(\vec{b}^2)$. The expression for $S_o(s)$ is taken from the high energy behaviour of quantum field theory [1] and we shall use the crossing symmetric expression [4]

$$S_o(s) = \frac{s^c}{(\ell n\, s)^{c'}} + \frac{u^c}{(\ell n\, u)^{c'}} \qquad (3)$$

where u is the third Mandelstam variable. Note that $S_o(s)$ is complex.

The impact parameter dependence of the Pomeron is contained in $F(\vec{b}^2)$ for which various ansazt have been proposed that we want to discuss briefly. In the earlier analysis [4] $F(\vec{b}^2)$ was chosen to be proportional to the function $exp(-\lambda\sqrt{b^2+b_o^2})$. For such a function the calculated amplitude has the interesting feature that it gives one dip in the differential cross section (once the parameters are adjusted), but it suffers from a fast decrease at large t and it is below the recent ISR data by a few orders of magnitude. Another ansazt follows from the proportionality between the charge density of the proton and the internal distribution of matter [6, 7]. If this proportionality is assumed to be exact, and a multipole approximation is used for the electromagnetic form factor of the proton, then the resulting amplitude gives a fair description of the differential cross section at ISR energies up to 2 GeV^2, but gives also around $|t| \sim 4$ GeV^2 a second dip, which is not observed at ISR.

Here we present a solution which overcomes the difficulties mentioned above by supposing that $\tilde{F}(t)$ is not only proportional to the square of the form factor, but also proportional to a slowly varying function of t which has a real zero. This possibility is not ruled out by quantum field theory, since the relation between $\tilde{F}(t)$ and the electromagnetic form factor is not exact [9]. We shall take

$$\tilde{F}(t) = f_\cdot [G(t)]^2 \cdot \frac{a^2+t}{a^2-t} \qquad (4)$$

with $$G(t) = \frac{1}{\left(1 - \frac{t}{m_1^2}\right)\left(1 - \frac{t}{m_2^2}\right)} \qquad (5)$$

The term G(t) corresponds to a reasonable parametrization of the form factor, while the last factor in (4) represents an approximation to the remaining t-dependence which is unknown at present. More elaborate expressions can be used provided they give a zero at a similar t value, but the function we propose involves only one free parameter and is a very simple one. Let us stress that with the slowly varying function introduced in Eq. (4) factorization is violated since it cannot be expressed as a product of vertex functions unless new branch cut singularities occur. However our Pomeron is a fixed cut so we do not need to preserve factorization.

Since we are interested in the analysis of low energy data we must add a spin independent Regge background that we shall take as

$$\widetilde{R}_0(s,t) = \left[C_+ + C_- e^{-i\pi\alpha(t)} \right] s^{\alpha(t)} \qquad (6)$$

representing the standard even and odd signature exchange contributions, with an exchange degenerate trajectory $\alpha(t) = \alpha_0 + \alpha' t$.

Notice that in ref. [4] only the energy dependence of σ_{tot} was fitted so a simple term as $A/\sqrt{s}$ was used instead of this Regge contribution.

Summarizing all the above expressions Eqs. (3) - (6) , we get :

$$\widetilde{\Omega}_0(s,t) = S_0(s)\,\widetilde{F}(t) + \widetilde{R}_0(s,t) \qquad (7)$$

whose Fourier transform provides $\Omega_0(s,b)$ from which one can calculate the spin independent amplitude

$$a_0(s,t) = \frac{s}{4\pi} \int_0^\infty J_0(b\sqrt{-t})\left(1 - e^{-\Omega_0(s,b)}\right) b\, db \qquad (8)$$

III - NUMERICAL RESULTS

The amplitude a_s involves 10 parameters that we fitted by taking the $\bar{p}p$ total cross section data and the elastic pp data on σ_{Tot}, $\rho = Re\, a_s / Im\, a_s$, and $d\sigma/dt$ in the momentum range from 14 GeV/c up to 2.000 GeV/c. As a result of the fit we have obtained the following values

$$c = 0.151 \qquad c' = 0.756 \qquad m_1 = 0.619 \text{ GeV} \qquad m_2 = 1.587 \text{ GeV}$$

$$a = 2.257 \text{ GeV} \qquad f = 8.125$$

$$C_+ = -39. \qquad C_- = 1.8 \qquad \alpha(t) = 0.352 + 0.694\, t \qquad (9)$$

with t in units of $(GeV)^2$. The asymptotic energy regime of hadronic interactions is controlled by c and c' and the above values obtained by using a very large set of data are more accurate than those from the previous determination [4].

A comparison of the model with experimental data is displayed in Figs. 1-9, and let us now discuss the results in some details. The double pole term $G(t)$ in Eq.(5) can be interpreted as the "form factor". In Fig. 1, $G(t)$ is plotted versus $-t$ with the values of m_1 and m_2 fitted from the differential cross section, the curve has the correct shape compared with the experimental electromagnetic form factor [10], however for large t it lies above the data points. Since we do not expect an exact connection with the form factor [9] we consider that this double pole parametrization is an approximate fit to the form factor.

The profile functions are shown in Fig. 2. The curve labelled $\Omega_G(b)$ represents the Fourier transform of $f \cdot [G(t)]^2$ and we observe that the introduction of a zero in Eq.(4) flattens the curve $F(b^2)$ in the low b region. Such a difference is necessary to reproduce correctly the large t behaviour of the cross section. A similar flattening effect has been obtained in a model of the quark-glue structure of the proton by Van Hove [15], who assumes that the glue amplitude is close to the unitarity limit at small impact parameter distance.

The total cross sections σ_{Tot} and the ratio $\rho = Re\, a_s / Im\, a_s$ are presented in Fig. 3, 4 as a check of the forward values of the amplitude. The Figures 5-8 show the fair agreement of the model with the differential cross section between 14 and 2000 GeV/c, in particular at $p_{Lab} = 1480$ GeV/c (see Fig. 7) we get the correct slope of the cross

section up to $|t| = 10$ GeV^2 and no second dip arises at such energy. However we observe a change of slope around $|t| = 8$ GeV^2 which might be a sign that a new dip develops at super high energies as pointed out by Chou and Yang [16]. We have also checked the energy dependence at fixed t ($-t = 6$ GeV^2) in Fig. 9, the curve reproduces the general trend of the data and we predict that the cross section is decreasing slowly with energy above $\sqrt{s} = 70$ GeV. For $\sqrt{s} < 25$ GeV where the Regge background is important, we observe that the theoretical curve lies below the data. This means that, for large $|t|$ around 6 GeV^2, the simple Regge contribution that we have used decreases too rapidly. As a possible further test of this Regge background, we plan in the future to calculate from the present phenomenology the case of antiproton-proton scattering, where no new parameter is needed. Possible significant deviations between the theory and the data may give valuable information about the Regge terms.

In view of the energy domain accessible to the future accelerators (Isabelle), Fig. 10 shows predictions at $\sqrt{s} = 200$ and 800 GeV.

IV - SPIN STRUCTURE OF THE MODEL

Up to now we have ignored the proton spin because the data we have analyzed are not sensitive to this degree of freedom. In the following we will show that with some simple hypothesis concerning the structure of the proton we are able to construct a spin dependent amplitude and then to calculate the polarization and the R parameter at different energies.

The concept of matter current inside a hadron is due to Chou and Yang [8]. They study the existence of a hadronic matter current inside a polarized hadron as a complementary aspect of their original hypothesis on hadronic matter density, the two concepts being analogous to the electromagnetic charge and current densities. As a consequence of their hypothesis, the presence of an hadronic matter current makes the interaction spin dependent and this leads to specific predictions on spin correlation parameters in particular the R parameter [8].

Let us assume that the scattering of two protons occurs in the x-y plane with the direction of the incident proton along the y-axis. Consider a small region of the target and call v_y the y component of the velocity of this region in the c.m. system of this region and of the projectile. The effective energy of the projectile in the rest system region of the target is :

$$s_{eff} = s(1 - v_y) \tag{10}$$

where higher order terms in v_y have been neglected. From Eq.(3) the energy dependence of the Pomeron exchange becomes now

$$S_o(s) \rightarrow S(s,\vec{b}) = S_o(s_{eff}) \sim S_o(s) - s v_y \frac{\partial}{\partial s} S_o(s)$$
$$= \frac{s^c}{(\ln s)^{c'}} - s v_y \frac{\partial}{\partial s} \frac{s^c}{(\ln s)^{c'}} + \text{cross terms in } u \tag{11}$$

The quantity v_y describes the motion of hadronic matter inside a proton, and is determined in a complicated way by strong interactions. For the present purposes, we propose to proceed with the simplest possible assumptions. In this section, we consider the case of rigid rotation

$$v_y = \omega b_x = \omega \hat{b}_x b \tag{12}$$

where ω is the angular velocity of the rigid rotation $\hat{b} = \vec{b}/b$ is a unit vector, and $\hat{b}_x$ is the x-component of $\hat{b}$.

Since rigid rotation is specified by only one parameter ω , it is the simplest conceivable assumption but it clearly has qualitatively undesirable features. Thus in the next section we shall consider a somewhat more complicated form of v_y .

From (11) and (12) we obtain

$$S(s,\vec{b}) = S_o(s) - \omega \hat{b}_x b \, S_1(s) \tag{13}$$

where

$$S_1(s) = \frac{s^c}{(\ln s)^{c'}} \left(c - \frac{c'}{\ln s} \right) + \frac{u^c}{(\ln u)^{c'}} \left(c - \frac{c'}{\ln u} \right)$$

The sign of v_y is related to the spin orientation of the target so we have

$$S(s,\vec{b}) = S_o(s) \mp \omega \hat{b}_x b \, S_1(s) \tag{13'}$$

where $\mp$ for target spin $\pm$ 1/2 along the z-axis.

We differ from the pioneering work of Chou and Yang [8] in two respects. First, their hadronic matter motion is not described by (12) ; and secondly, because $S(s,\vec{b})$ as given by (13) is complex, we get a non-vanishing polarization at high energies when the pomeron dominates.

The total opaqueness $\Omega(s,\vec{b})$ which occurs in Eq.(1) is obtained in this case from Eq.(2) by the substitution $S_0(s) \to S(s,\vec{b})$ given by Eq.(13') which yields

$$\Omega(s,\vec{b}) = \Omega_0(s,b) \mp \Omega_1(s,b)\,\hat{b}_x \qquad (14)$$

with

$$\Omega_1(s,b) = F_s(\vec{b}^2)\,S_1(s) + R_1(s,b) \qquad (15)$$

where $F_s(\vec{b}^2) = b\,\omega\,F(\vec{b}^2)$ and $R_1(s,b)$ is a necessary Regge spin dependent contribution in order to study polarization and rotation parameters at low energies. More explicitly, $R_1(s,b)$ is the Fourier transform of the standard Regge background

$$\tilde{R}_1(s,t) = \sqrt{-t}\,\left[c'_+ + c'_-\, e^{-i\pi\alpha(t)}\right] e^{Bt}\, s^{\alpha(t)} \qquad (16)$$

which has the appropriate kinematical factor $\sqrt{-t}$ and an exponential damping factor in the residue. This damping factor which should be included in general was not necessary for the spin independent amplitude $a_0(s,t)$ (see also ref. 17).

The total scattering amplitude defined by Eq.(1) can be written as

$$M(s,t) = a_0(s,t) + i\,\vec{\sigma}\cdot\vec{n}\; a_1(s,t) \qquad (17)$$

where $\vec{n}$ is a unit vector normal to the scattering plane, $a_0(s,t)$ is given by Eq.(8) and the spin dependent amplitude $a_1(s,t)$ reads

$$a_1(s,t) = i s \int_0^\infty J_1\left(b\sqrt{-t}\right)\Omega_1(s,b)\, e^{-\Omega_0(s,b)}\, b\,db \qquad (18)$$

where the Bessel function J_1 comes from the angular integration.

In addition we have included the real contribution of one-photon exchange to the scattering amplitudes a_0 and a_1 which leads to a sizeable effect in the polarization at high energies and large momentum transfer (see ref. 18).

Let us finally recall the expressions in terms of the amplitude $a_0(s,t)$ and $a_1(s,t)$ of the four observables in the laboratory system corresponding to the scattering with a polarized proton target. These observables are :

$$\sigma_0 = |a_0|^2 + |a_1|^2 \tag{19}$$

$$\sigma_0 P = 2\, Im\,(a_0 a_1^*) \tag{20}$$

$$\sigma_0 R_{Lab} = -\left(|a_0|^2 - |a_1|^2\right)\cos(\theta - \theta_R) - 2\,Re\,(a_0 a_1^*)\sin(\theta - \theta_R) \tag{21}$$

$$\sigma_0 A_{Lab} = -\left(|a_0|^2 - |a_1|^2\right)\sin(\theta - \theta_R) + 2\,Re\,(a_0 a_1^*)\cos(\theta - \theta_R) \tag{22}$$

where θ is the center of mass scattering angle, θ_R is the recoil angle in the laboratory system.

V - SPIN STRUCTURE OF THE MODEL (CONTINUED)

Although rigid rotation involves the least number of parameters, it is unsatisfactory from a theoretical point of view for the following reason. Consider the mathematical limit of $s \to \infty$, where contributions from large impact parameter become very important. If (12) is taken literally, matter velocity is proportional to the impact parameter, and thus there is significant violation of special relativity in exceeding the velocity of light. It is much more reasonable to assume that the momentum density, instead of the matter velocity, is proportional to the impact parameter. If so, the important contribution to rotation parameters, in the limit $s \to \infty$, comes from hadronic matter moving at nearly the velocity of light. This situation is still not plausible.

The simplest way to avoid this problem is to replace ω, the angular velocity for rigid rotation, by $\omega(b^2)$, a function of the impact parameter chosen such that

$$\omega(b^2) \longrightarrow 0 \tag{23}$$

as $b^2 \to \infty$. In contrast to rigid rotation, such motion will be referred to as soft rotation.

This replacement of $\omega \rightarrow \omega(b^2)$ should be carried out for all the formulas of the last section. Thus, for example, eq.(13) is now

$$S(s,b) = S_0(s) - \omega(b^2)\,\hat{b}_x\, b\, S_1(s) \qquad (24)$$

and the $F_s(\vec{b}^2)$ of (15) is given by

$$F_s(\vec{b}^2) = b\,\omega(b^2)\,F(\vec{b}^2) \qquad (25)$$

Even though this generalization of introducing a function of the impact parameter is completely straightforward, we must be aware of the complications of this generalization. Rigid rotation has the following character. Consider a proton executing rigid rotation about the z-axis, then for a given value of b_x the y-component of the velocity is independent of b_y, and is given by (12). For soft rotation, this is no longer true. In other words, for soft rotation about the z-axis, the y-component of the velocity depends not only on b_x but also b_y. Therefore, in the impact parameter representation, the effective energy of the collision varies as the projectile passes through the target, and hence the s_{eff} of eq.(10) has a spread.

We choose to ignore this complication for the present phenomenological analysis. The reason is that at present very little is known about hadronic matter current, and that soft rotation is only meant to describe the gross features of this current. It thus seems reasonable to view s_{eff} as an average of the effective values of s as the projectile passes through the target, and v_y as an average value of the velocities for a given value of b_x. In the future, when hadronic matter current is better understood, it will be necessary to study such complications in detail, and it is likely that physical effects may be directly measured.

VI - POLARIZATION AND R PARAMETER

We shall discuss the results in the two cases considered above.

a) Rigid rotation.

The parametrization of the flip amplitude involves four parameters ω , $C_{\pm}^{\downarrow}$, B . The fit of the polarization data between 17-100 GeV/c shows that the value of the parameter ω in the Pomeron exchange is ω = - 0.06 GeV. The Regge flip parameters are $C_{+}^{\downarrow}$ = 11.246 , $C_{-}^{\downarrow}$ = - 7.623, B = 1.942 GeV^{-2} and $\alpha(t)$ is the same as the non flip. We present the results for the polarization at p_{lab} = 100 GeV/c compared with the data on Fig. 11. A prediction for P at p_{lab} = 300 GeV/c is given on Fig. 12 and shows large positive values in the dip region. We have calculated the R parameter at different energies 100, 280 and 1480 GeV/c shown in Fig. 13.

The results on the R parameter have been reported elsewhere [20] .

b) Soft rotation.

Besides the condition (23), there is no guidance in selecting the function $\omega(b^2)$. We choose, rather arbitrarily, the gaussian form

$$\omega(b^2) = \omega_o \, e^{-b^2/b_o^2} \qquad (26)$$

where one additional parameter, b_0 , has been introduced. Another plausible form is

$$\omega(b^2) = \omega_o \, \frac{b_o^2}{b^2 + b_o^2} \qquad (27)$$

With (26), we have five parameters in that case whose values are : ω_o = - 0.06 GeV, b_0 = 3.75 GeV^{-1} . The Regge flip parameters are $C_{+}^{\downarrow}$ = 3.547, $C_{-}^{\downarrow}$ = - 1.538, B = 0.597 GeV^{-2} . With these parameters the profile function $F_s(\vec{b}^2)$ which corresponds to the spin dependent part of the Pomeron is plotted in Fig. 2 and as expected it exhibits a peripheral behaviour.

The results on the polarization are in Figs. 14, 15, 16 for

the energies 17.5 , 45 and 100 GeV/c, there is a good agreement with experiments in particular at low t values. There is also preliminary data from FNAL at high energy and fixed t value ($|t| = 0.3$ GeV^2), our results are compatible with the present data, see Fig. 17. We also present on Figs. 18 and 19 predictions of our model for $p_{lab} = 150$ and 300 GeV/c which will be soon compared with new experimental data.

We have calculated the R parameter at different energies : 45 , 100 , 280 and 1480 GeV/c in Figs. 20 - 22. In order to emphasize the influence of a_1 , on R_{Lab} we plotted at 45 GeV/c a curve with no spin dependence ($a_1 = 0$). We observe that at low t ($-t \lesssim 0.5$ GeV^2) the spin effect is negligible, while for $-t \sim 1$ GeV^2 the two curves separate. The existing data at low t [23] have too large errors and so yield no precise conclusion. From our result,future experiments at large -t will be of interest for the detection of spin effect if reasonable errors are obtained. At FNAL or SPS energies, the R parameter develops a rapid variation between 100 and 300 GeV/c around $-t = 1.3$ GeV^2 at the position of the dip in the differential cross section (see fig.22). This effect can be detected, because we notice in Eq.(20), that if no spin effect was present R would behave as $\cos(\delta - \delta_R)$, so any departure from that curve indicates the presence of spin interference. Let us stress that for the energies above 200 GeV/c where the Regge background becomes negligible the predictions of our model for the Pomeron spin amplitude depend on two parameters ω_o and b_o for the case of soft rotation.

VI - CONCLUSION

We have presented a phenomenological analysis of pp elastic scattering from $p_{lab} = 17$ GeV/c up to 2000 GeV/c by means of a new impact picture with a specific spin dependence. The model derived from the asymptotic energy behaviour of relativistic quantum field theory gives a fair description of the data in particular at ISR energies and large momentum transfers. It shows that no significant modifications on our ideas on diffraction are necessary and contradicts the statement according to which eikonal models are inadequate for high energy processes [24] . The absence of a second dip at ISR energies [25] is due to the following facts i) the energy dependence of the Pomeron

is described by a complex function of energy $S(s)$, ii) the profile function $F(\vec{b}^2)$ is close to the unitarity limit near $b \sim 0$, and for large b decreases less rapidly than a gaussian. This flattening of $F(\vec{b}^2)$ at small b is produced by a zero at $|t| \sim 5$ GeV^2 in $\tilde{F}(t)$.

Once the phenomenologically satisfactory impact picture of Section 2 is available, it is then possible to study the spin dependence at high energies by combining the impact picture with the hadronic matter current of Chou and Yang [8]. Two of the simple possibilities are the cases of rigid rotation and soft rotation. While rigid rotation is the simplest in the sense of involving the least number of parameters, it has serious theoretical difficulties in the limit of infinite energy. Soft rotation, on the other hand, involves at least one more parameter but seems to have no conceptual difficulty.

For the two phenomenological models of rigid rotation and soft rotation, the predictions for both polarization and the R parameter are quite different. This means that these two models can be easily differentiated experimentally by measuring either the polarization or the R parameter. In view of the theoretical difficulty with the case of rigid rotation, we prefer the model of soft rotation. Whether this prejudice of ours is justified or not can probably be determined by experiments in the near future.

We have discussed in this paper on the case of proton-proton scattering. The ideas and the analysis can clearly be applied to many other two-body elastic scattering processes. In particular, recent measurements [26] show that the lambda-proton polarization is larger than the proton-proton polarization which might indicate that the matter inside a lambda rotates faster than in the case of a proton. In this connection, we mention our speculation about a possible connection between the angular velocity of rotation and the isoscalar magnetic moment [20].

In conclusion, we reiterate that the measurement of the R parameter at FNAL or CERN SPS will be an important test on the validity of the different pictures of the matter motion inside a proton, because several distinct theoretical predictions are now available.

ACKNOWLEDGEMENTS

We are greatly indebted to Professor O.E. Overseth for private communications on his measurement of lambda-proton polarization. One of us (TTW) thanks Professor C.N. Yang and Professor T.N. Truong for instructive discussions on hadronic matter motion, and is most grateful to members of the Instituut voor Theoretische Fysica at Utrecht, especially Professor Martinus J.G. Veltman, for their hospitality.

- REFERENCES -

[1] H. CHENG and T.T. WU,
Phys.Rev. D1, 2775 (1970) and
Phys.Rev.Letters 24, 1456 (1970)

[2] M. FROISSART,
Phys.Rev. 123, 1053 (1961)

A. MARTIN
Phys.Rev. 129, 1432 (1963) and
Nuovo Cimento 42, 930 (1966)

[3] U. AMALDI et al.,
Phys.Letters 44B, 112 (1973)

S. AMENDOLIA et al.,
Phys.Letters 44B, 119 (1973)

[4] H. CHENG, J. WALKER and T.T. WU,
Phys.Letters 44B, 97 (1973)

H. CHENG and T.T. WU,
High Energy Collisions, A.I.P. Conference Proceedings, n° 15
(Stony Brook 1973), edited by C. Quigg.

[5] T.T. WU,
Proceedings of the XVIIIth International Conference on High
Energy Physics, Tbilisi (1976) p. A5-23.

[6] T.T. WU and C.N. YANG,
Phys.Rev. 137, B708 (1965)

[7] T. CHOU and C.N. YANG,
Phys.Rev. 17C, 1591 (1968), ibidem 175, 1832 (1968)
Phys.Rev.Letters 20, 1213 (1968)

[8] T. CHOU and C.N. YANG,
Nucl. Phys. B107, 1 (1976)

[9] H. CHENG and T.T. WU,
Phys.Rev. 184, 1868 (1969)

[10] P. KIRK et al.,
Phys.Rev. D8, 63 (1973)

[11] J. ALLABY et al.,
Phys.Letters 30B, 500 (1979)

U. AMALDI et al.,
Phys.Letters 44B, 112 (1973), ibidem 62B, 460 (1976)

A. CARROLL et al.,
Phys.Letters 61B, 303 (1976)

S. DENISOV et al.,
Phys.Letters 36B, 415 and 529 (1971)

K. FOLEY et al.,
Phys.Rev.Letters 19, 857 (1967)

[12] U. AMALDI et al.,
Phys.Letters 43B, 231 (1973), ibidem 66B, 390 (1977)

V. BARTENEV et al.,
Phys.Rev.Letters 31, 1367 (1973)

G. BELLETINI et al.,
Phys.Letters 14, 164 (1965)

G. BEZNOGIKH et al.,
Phys.Letters 39B, 411 (1972)

[13] J. ALLABY et al.,
Nucl.Phys. B52, 316 (1973)

[14] N. KWAK et al.,
Phys. Letters 58B, 233 (1975)

H. de KERRET et al.,
Phys. Letters 62B, 363 (1976),
ibidem 68B, 374 (1977)

[15] L. VAN HOVE,
Nucl.Phys. B122, 525 (1977)

[16] T. CHOU and C.N. YANG,
Preprint ITP-SB-77-67

[17] C. BOURRELY, A. MARTIN, J. SOFFER and D. WRAY,
Journal of Physics G3, 295 (1977)

[18] C. BOURRELY and J. SOFFER,
Lettere al Nuovo Cimento 19, 569 (1977)

[19] R. KLINE et al.,
A.I.P. Conference Proceedings n° 35, 152 (1976), Ed. M. Marshak

[20] C. BOURRELY, J. SOFFER and T.T. WU,
Impact Picture for Polarization and Rotation Parameter in
High Energy Proton-Proton Scattering,
to be published in Phys. Letters B

[21] M. BORGHINI et al.,
Phys.Letters 31B, 405 (1970), ibidem 36B, 501 (1971)

[22] A. GAIDOT et al.,
Phys.Letters 61B, 103 (1976).

[23] J. PIERRARD et al.,
Phys. Letters 61B, 107 (1976)

[24] U. SUKHATME,
Phys.Rev.Letters 38, 124 (1977)

[25] The effect of inelastic diffraction can be used to fill in the second dip ; see

P. CROZIER and B. WEBBER,
Nucl.Phys. B115, 509 (1976) and Preprint HEP 77/4 (1977), Cambridge

R. HENZI and P. VALIN,
On the Diffractive Nature of Elastic Scattering,
Preprint McGill University, 1977.

[26] B. EDELMAN et al.,
Phys.Rev.Letters 40, 491 (1978)

- FIGURES CAPTIONS -

Fig. 1 Proton electromagnetic form factor $G_M(t)/\mu$ compared with the function $G(t)$ (Eq.(5)) (for a compilation, see ref. [10]).

Fig. 2 Profile functions. $\Omega_G(b)$ (solid curve) corresponds to the Fourier transform of $f.[G(t)]^2$, $F(\vec{b}^2)$ (dashed curve) to the transform of Eq.(4) and $F_s(\vec{b}^2)$ (dotted curve) is the spin dependent profile function corresponding to soft rotation.

Fig. 3 σ_{Tot} proton-proton and antiproton-proton (data are from ref. [11] and prediction for ISABELLE energies. The dashed curves are the predictions of ref. [4] with $c' = 0$.

Fig. 4 $\mathrm{Re}\, a_0/\mathrm{Im}\, a_0$ as a function of p_{lab} (data from ref. [12]).

Fig. 5 Differential cross section at $p_{lab} = 14.2$ GeV/c (data from ref. [13]).

Fig. 6 Differential cross section at $p_{lab} = 290$ GeV/c (data from ref. [14]).

Fig. 7 Differential cross section at $p_{lab} = 1480$ GeV/c (data from ref. [14]).

Fig. 8 Differential cross section at $p_{lab} = 2060$ GeV/c (data from ref. [14]).

Fig. 9 Differential cross section as a function of $\sqrt{s}$ and fixed $-t = 6$ GeV^2.

Fig. 10 Differential cross section at $\sqrt{s} = 200$ and 800 GeV.

Fig. 11 Polarization at 100 GeV/c (data from ref. [19]) (rigid rotation).

Fig. 12 Polarization at 300 GeV/c (rigid rotation).

Fig. 13 Predictions of R_{Lab} at 100, 280, 1480 GeV/c (rigid rotation).

Fig. 14 Polarization at 17.5 GeV/c (data from ref. [21]).

Fig. 15 Polarization at 45 GeV/c (data from ref. [22]).

Fig. 16 Polarization at 100 GeV/c (data from ref. [19]), the dashed curve provides our prediction when the Coulomb contribution is not included.

Fig. 17 Polarization as a function of s for fixed $-t = 0.3$ GeV^2.

Fig. 18 Polarization at 150 GeV/c, the dashed curve provides our prediction when the Coulomb contribution is not included.

Fig. 19 Polarization at 300 GeV/c, the dashed curve provides our prediction when the Coulomb contribution is not included.

- FIGURES CAPTIONS (continued) -

Fig. 20 R_{Lab} at p_{lab} = 45 GeV/c (data from ref. [23]). Solid curve model prediction. Dashed curve model prediction with no spin ($a_1 = 0$).

Fig. 21 Predictions of R_{Lab} at 150, 300, 1480 GeV/c.

Fig. 22 Predictions of R_{Lab} at 100, 200, 300 GeV/c for $1.3 < |t| < 1.7$ GeV^2.

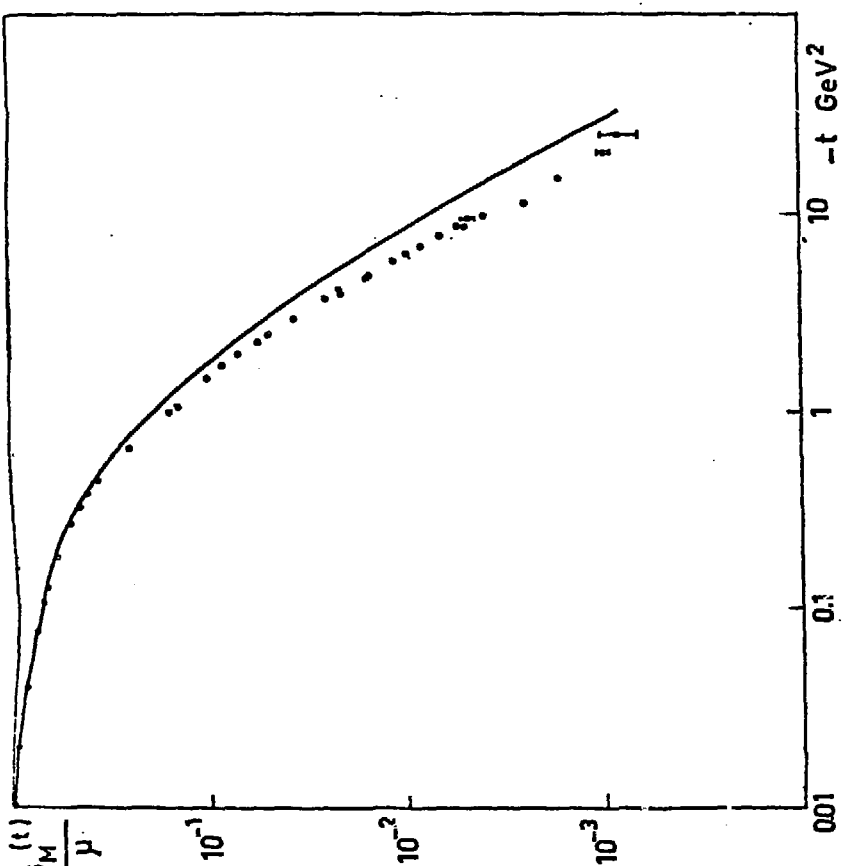

Fig. 1

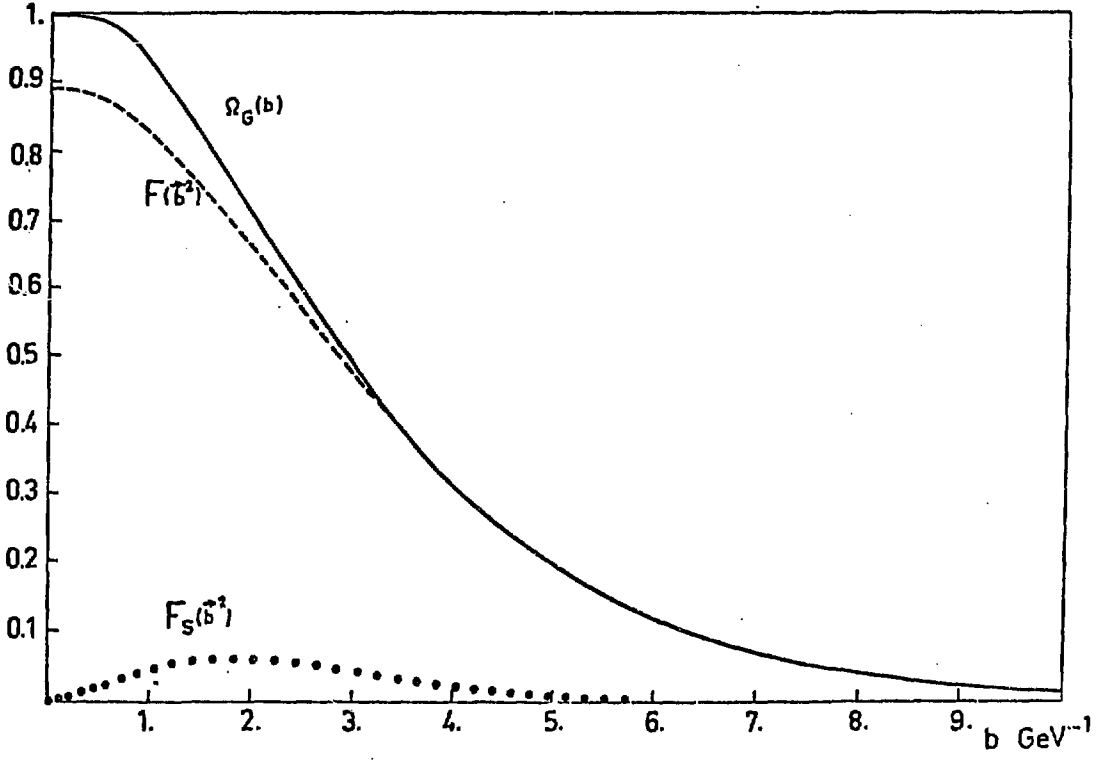
1.
0.9
0.8
0.7
0.6
0.5
0.4
0.3
0.2
0.1
$\Omega_G(b)$
$F(\vec{b}^2)$
$F_S(\vec{b}^2)$
1.
2.
3.
4.
5.
6.
7.
8.
9.
b GeV^{-1}

Fig. 2

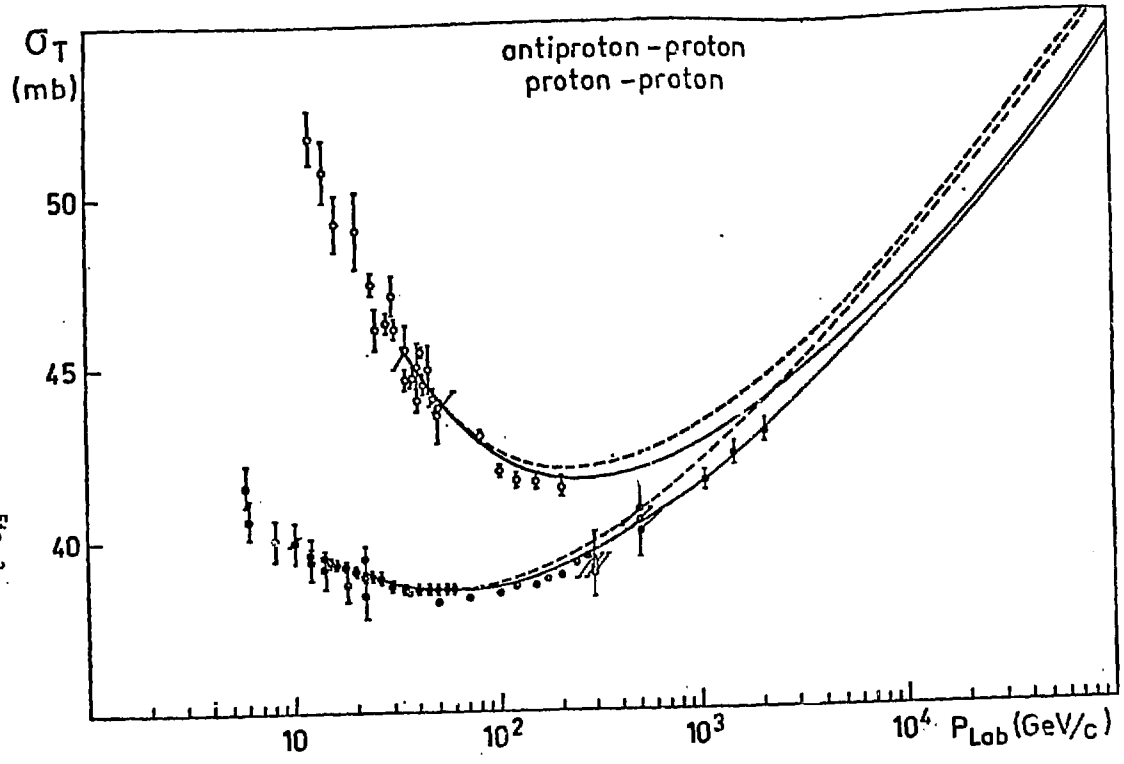
σ_T (mb)
antiproton - proton
proton - proton
50
45
40
10
10^2
10^3
10^4
P_{Lab} (GeV/c)

Fig. 3

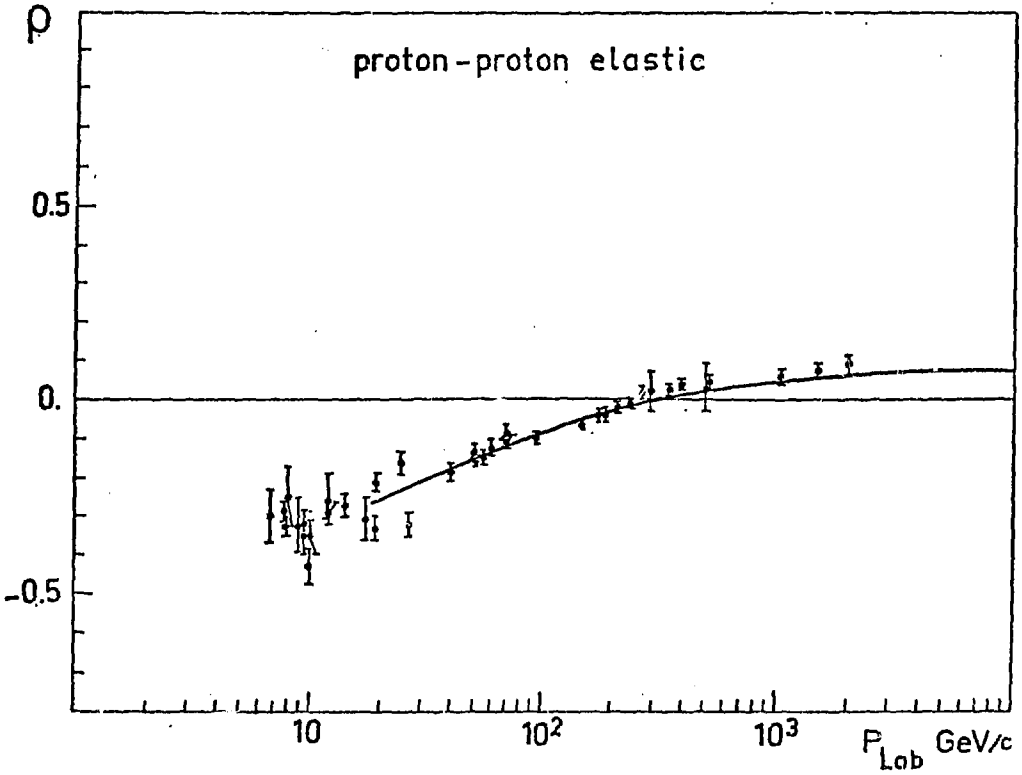

Fig. 4

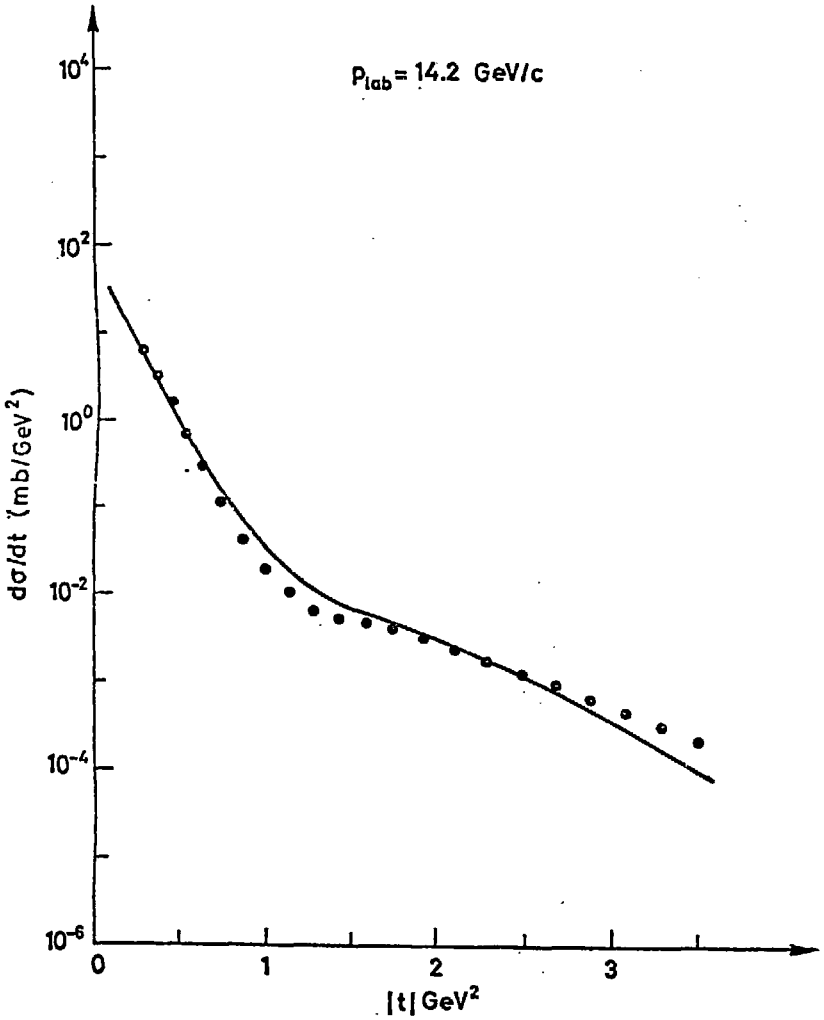

Fig. 5

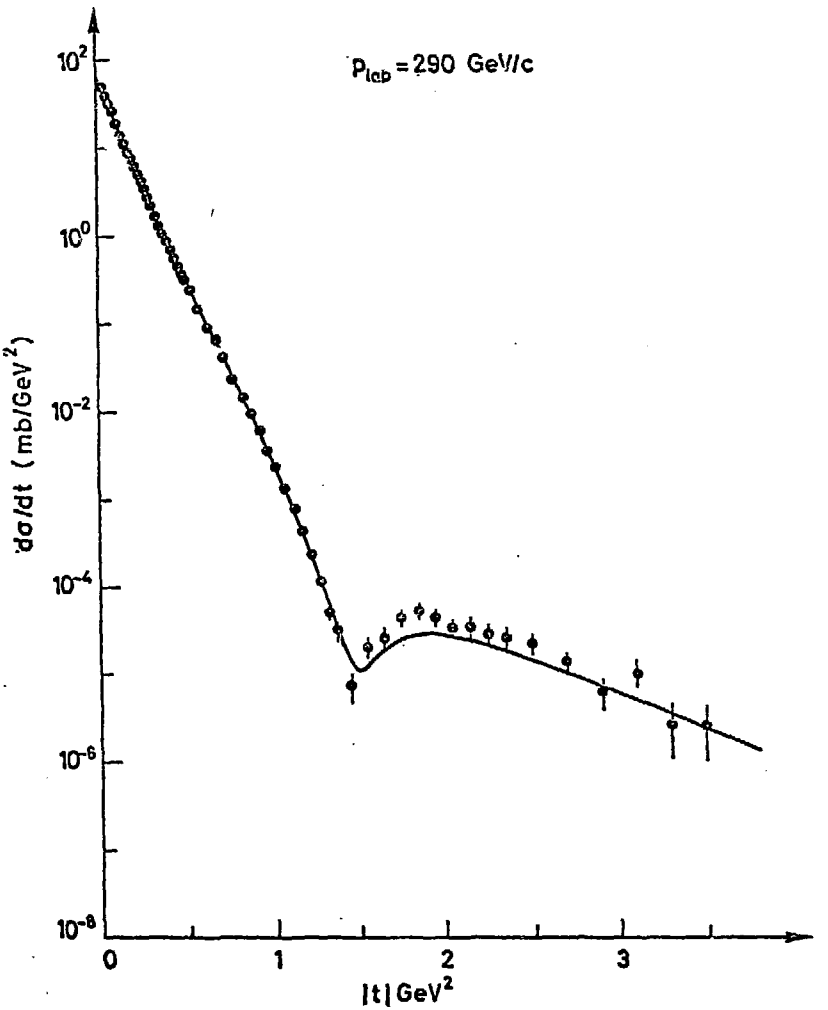
$p_{lab} = 290$ GeV/c
10^2
10^0
10^{-2}
10^{-4}
10^{-6}
10^{-8}
$d\sigma/dt$ (mb/GeV^2)
0
1
2
3
$|t|$ GeV^2

Fig. 6

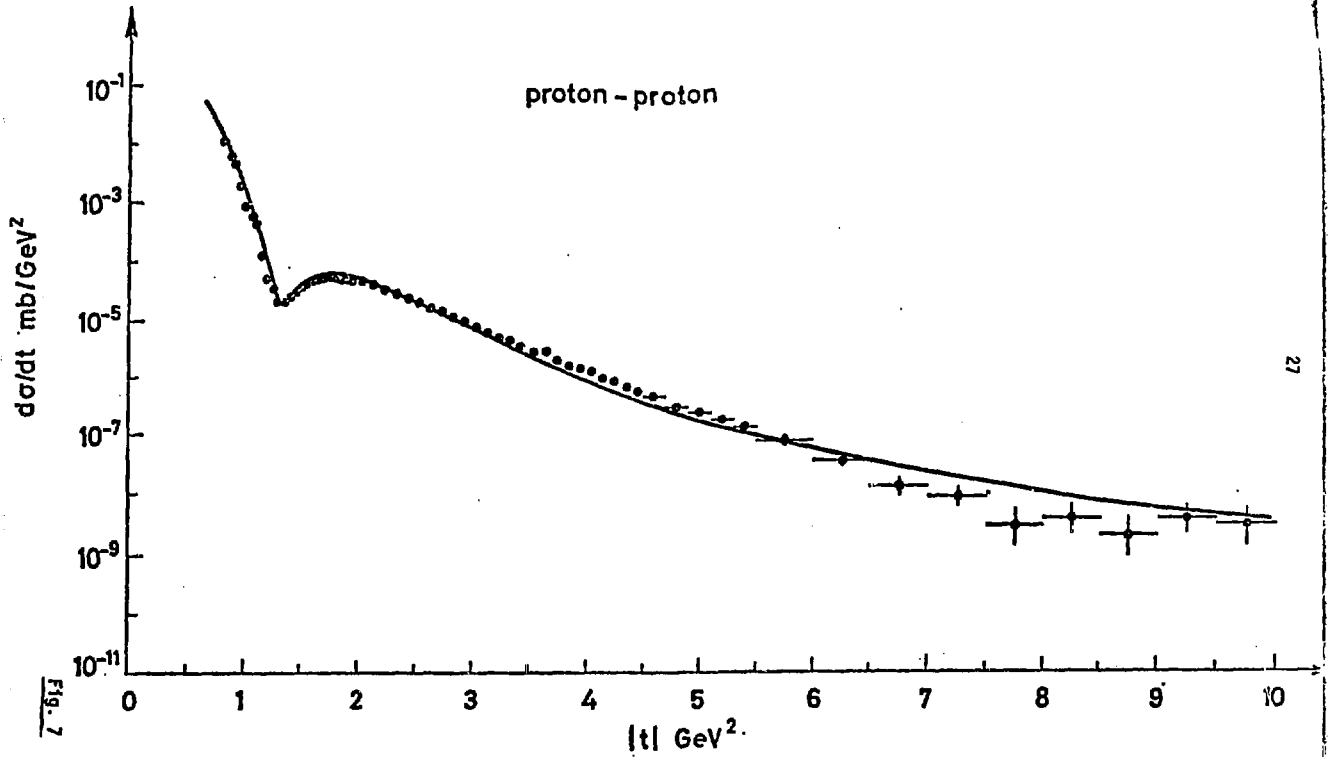
proton – proton
dσ/dt mb/GeV²
10⁻¹
10⁻³
10⁻⁵
10⁻⁷
10⁻⁹
10⁻¹¹
0
1
2
3
4
5
6
7
8
9
10
|t| GeV².

Fig. 7

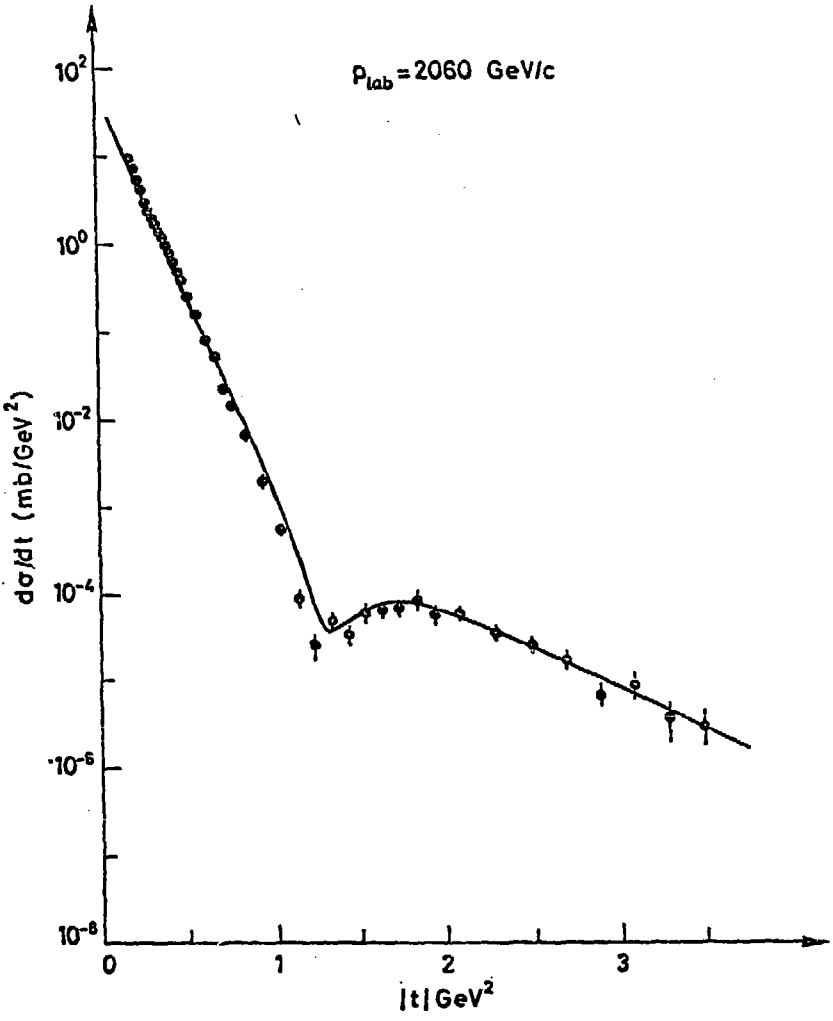
$p_{lab} = 2060$ GeV/c
10^2
10^0
10^{-2}
10^{-4}
10^{-6}
10^{-8}
$d\sigma/dt$ (mb/GeV^2)
0
1
2
3
$|t|$ GeV^2

Fig. 8

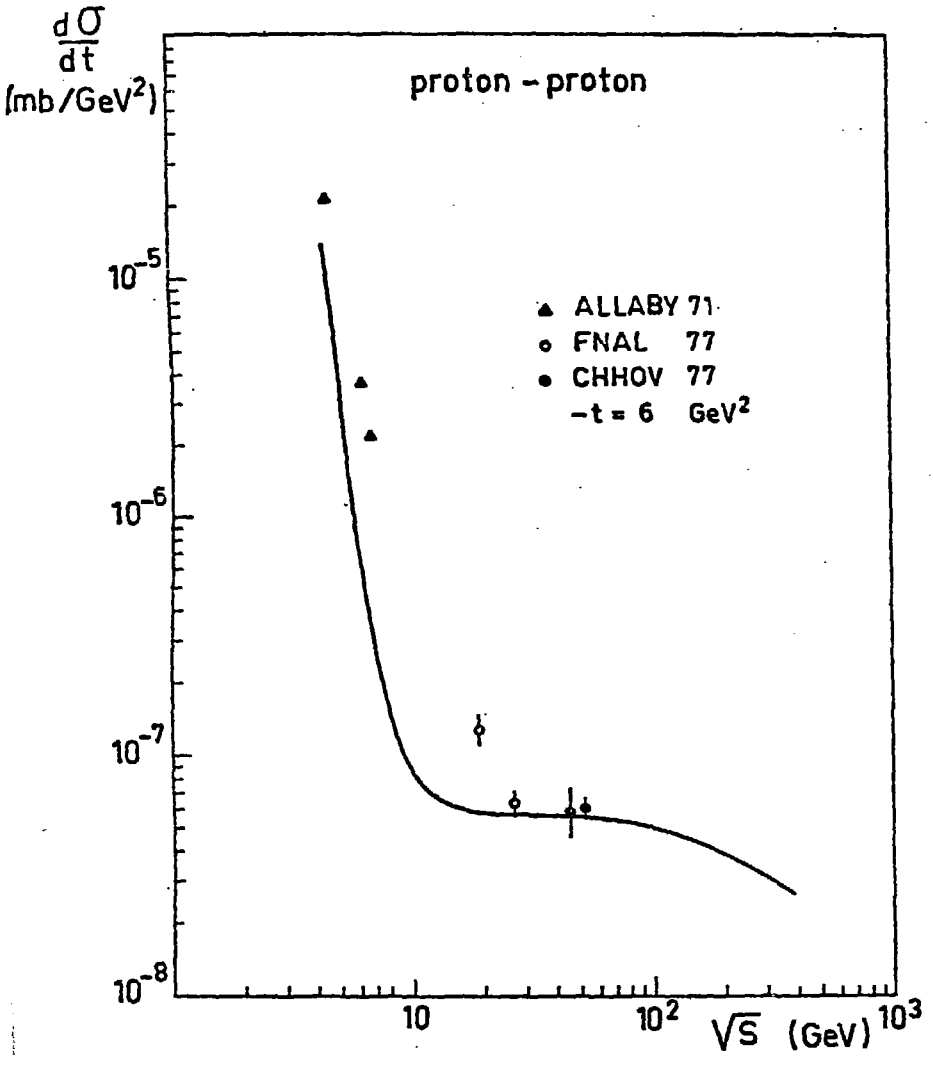
dσ/dt (mb/GeV²)
proton – proton
ALLABY 71
FNAL 77
CHHOV 77
–t = 6 GeV²
10⁻⁵
10⁻⁶
10⁻⁷
10⁻⁸
10
10²
√s (GeV)
10³

Fig. 9

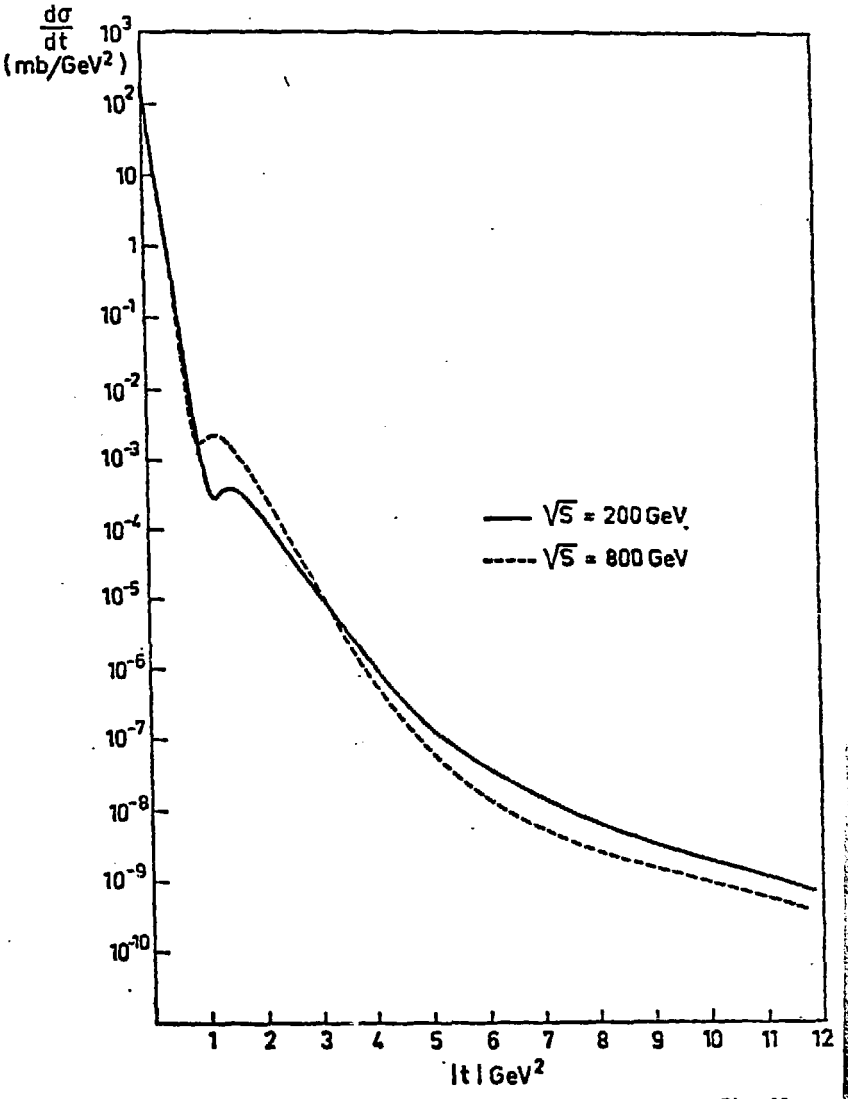
dσ/dt (mb/GeV²)
10³
10²
10
1
10⁻¹
10⁻²
10⁻³
10⁻⁴
10⁻⁵
10⁻⁶
10⁻⁷
10⁻⁸
10⁻⁹
10⁻¹⁰
√S = 200 GeV
√S = 800 GeV
1 2 3 4 5 6 7 8 9 10 11 12
|t| GeV²

Fig. 10

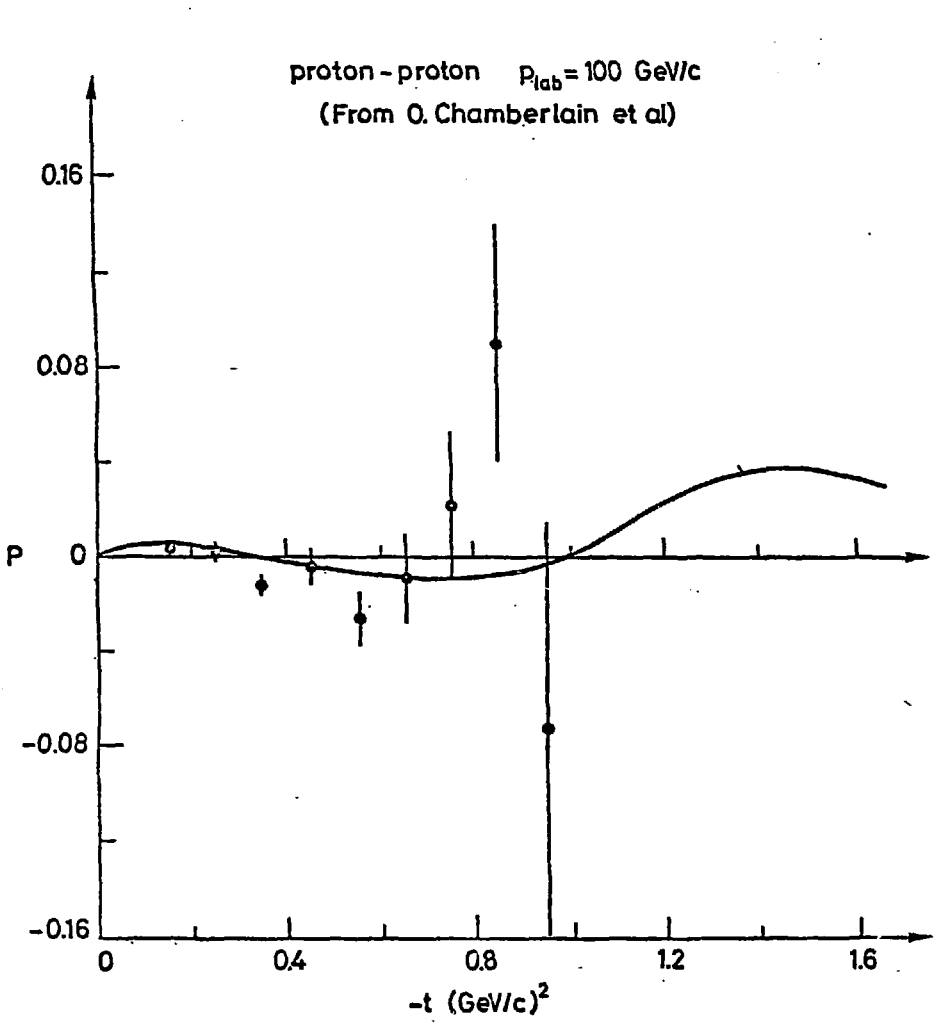
proton - proton p_{lab} = 100 GeV/c
(From O. Chamberlain et al)
0.16
0.08
P 0
-0.08
-0.16
0
0.4
0.8
1.2
1.6
-t (GeV/c)^2

Fig. 11

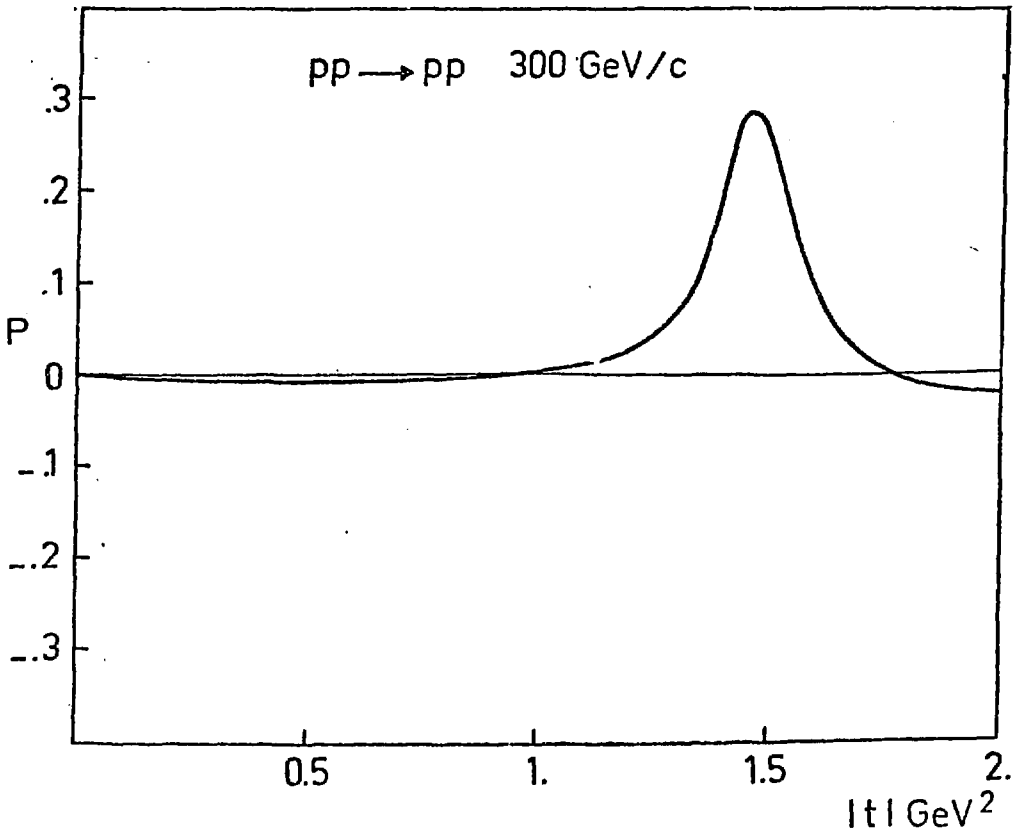

Fig. 12

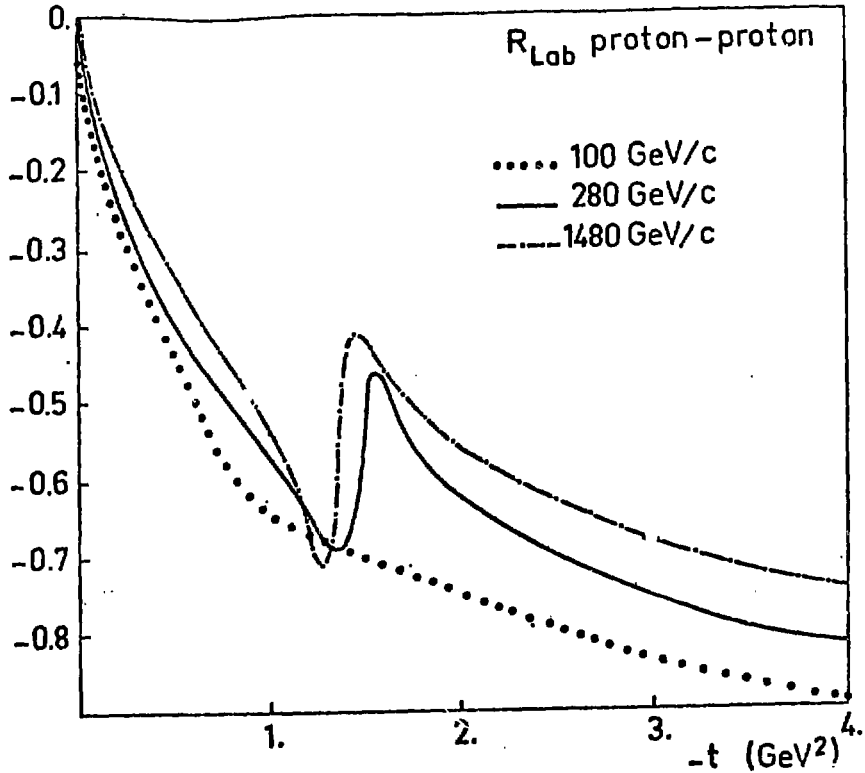
R_{Lab} proton – proton
100 GeV/c
280 GeV/c
1480 GeV/c
0.
-0.1
-0.2
-0.3
-0.4
-0.5
-0.6
-0.7
-0.8
1.
2.
3.
4.
-t (GeV²)

Fig. 13

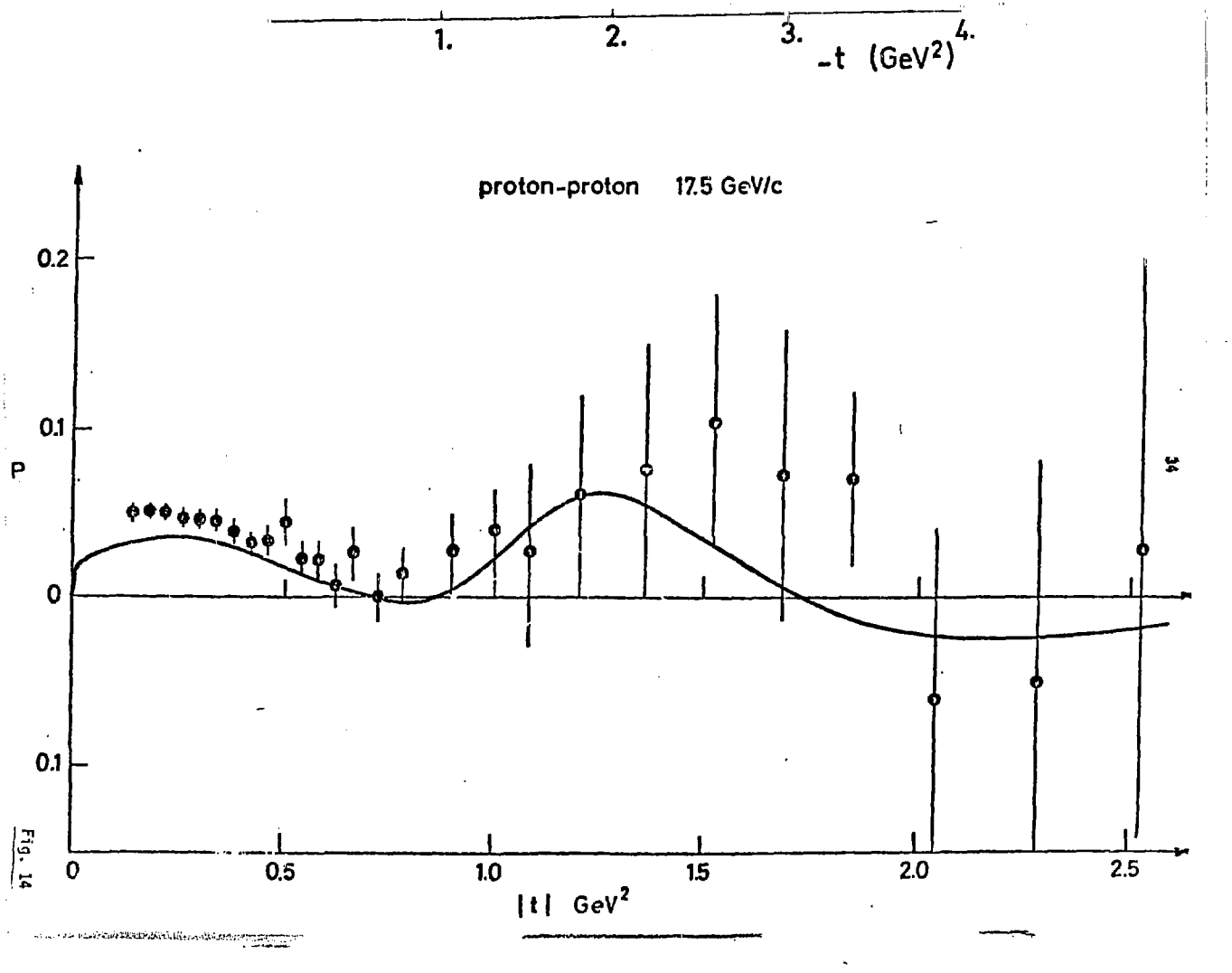
1.
2.
3.
4.
-t (GeV²)
proton-proton 17.5 GeV/c
0.2
0.1
P
0
0.1
0
0.5
1.0
1.5
2.0
2.5
|t| GeV²

Fig. 14

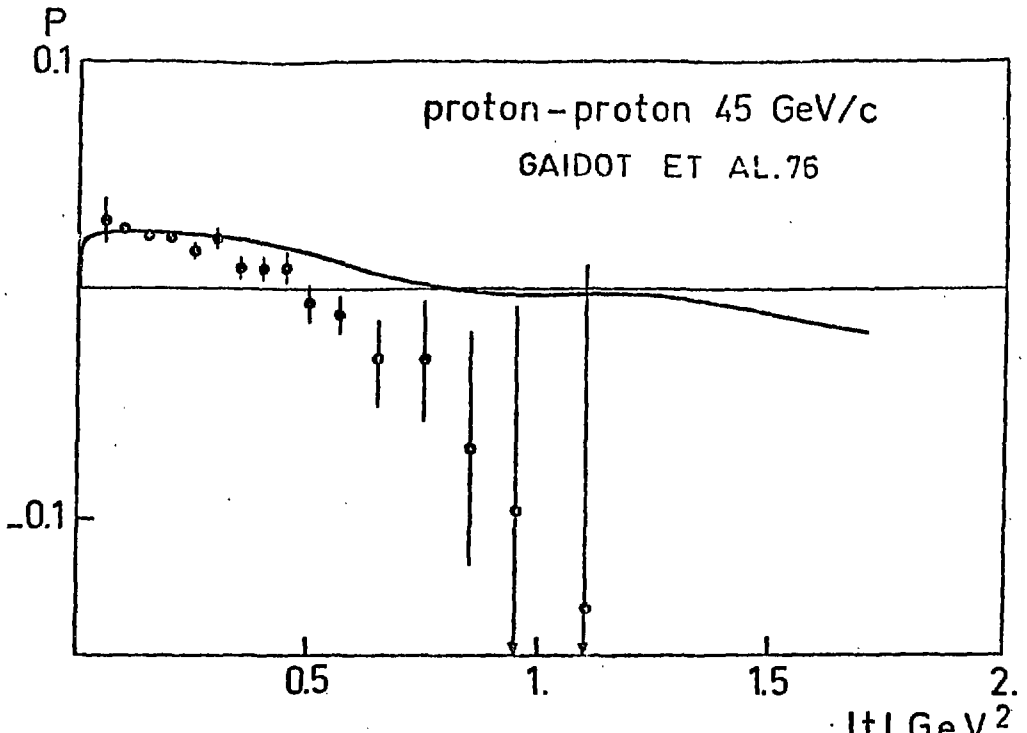

Fig. 15

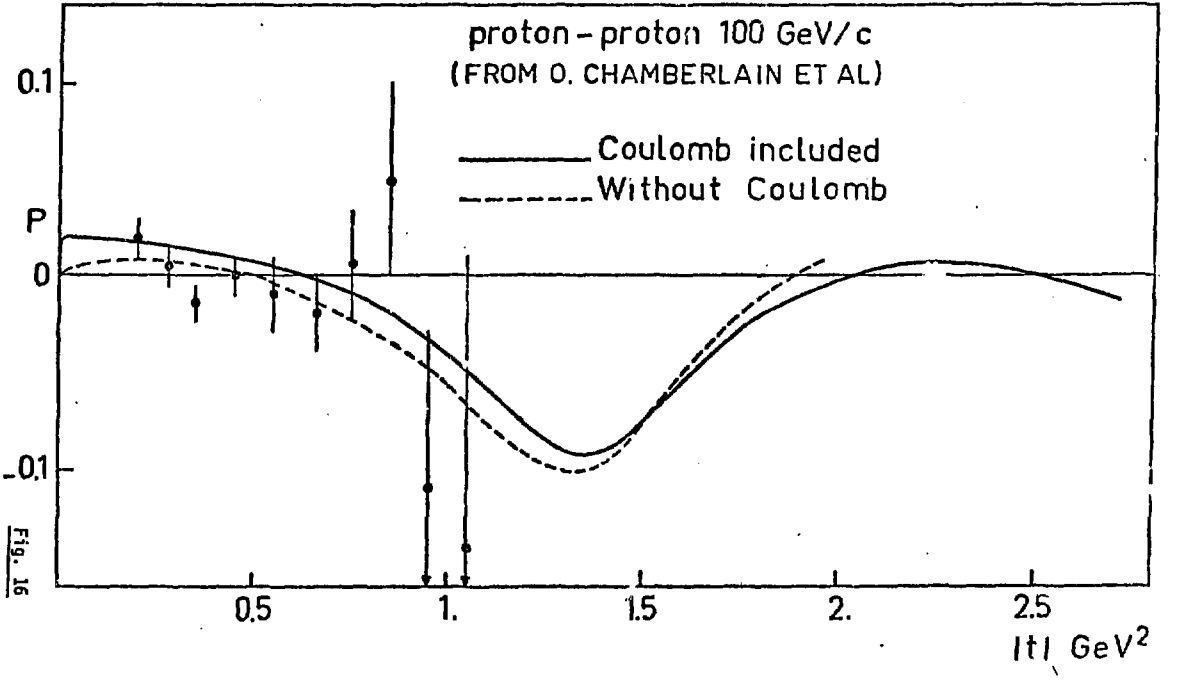
proton - proton 100 GeV/c
(FROM O. CHAMBERLAIN ET AL)
Coulomb included
Without Coulomb
P
0.1
0
-0.1
0.5
1.
1.5
2.
2.5
|t| GeV²

Fig. 16

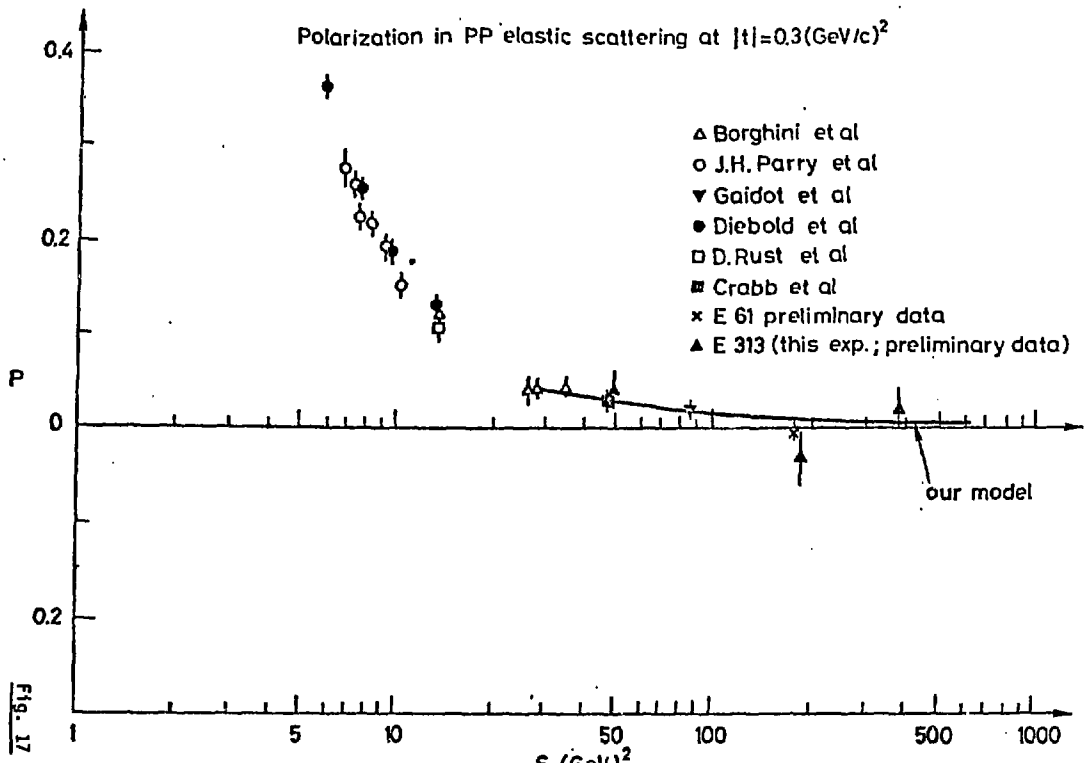
Polarization in PP elastic scattering at |t|=0.3(GeV/c)²
Δ Borghini et al
o J.H. Parry et al
▼ Gaidot et al
● Diebold et al
□ D. Rust et al
■ Crabb et al
× E 61 preliminary data
▲ E 313 (this exp.; preliminary data)
our model
P
0.4
0.2
0
0.2
1
5
10
50
100
500
1000
S (GeV)²

Fig. 17

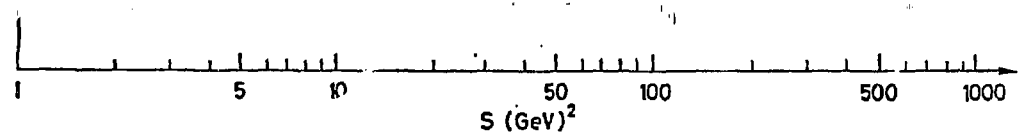
1
5
10
50
100
500
1000
S (GeV)²

Fig. 17

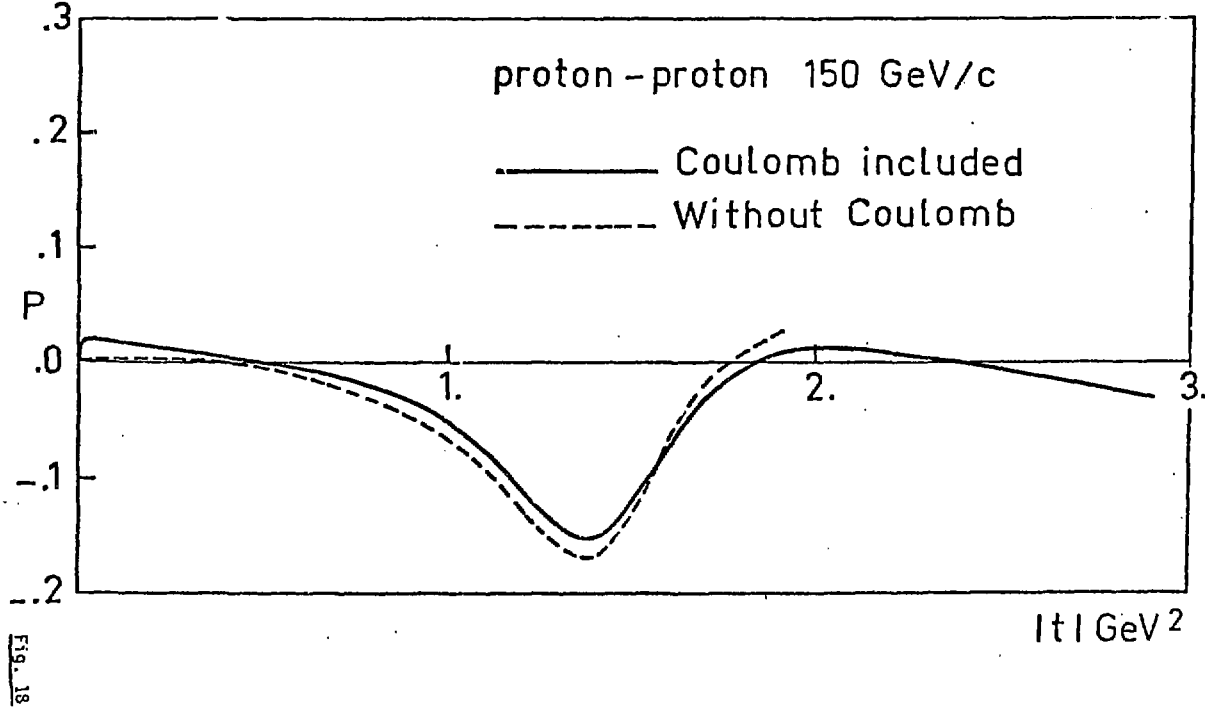
proton – proton 150 GeV/c
Coulomb included
Without Coulomb
P
.3
.2
.1
.0
-.1
-.2
1.
2.
3.
|t| GeV²

Fig. 18

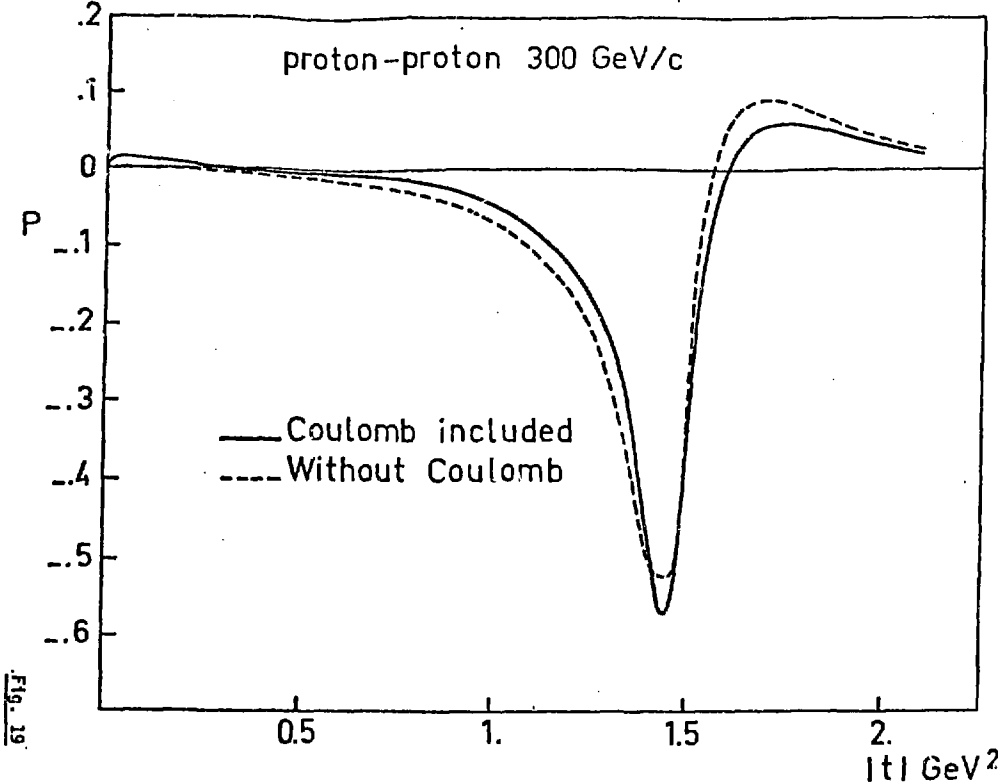

Fig. 19

0.1

R_{lab} proton - proton

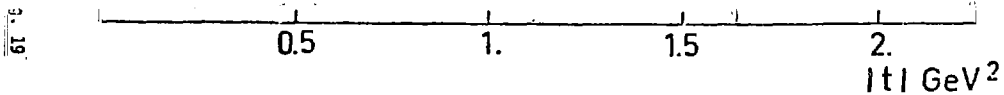
0.5
1.
1.5
2.
|t| GeV²

Fig. 19

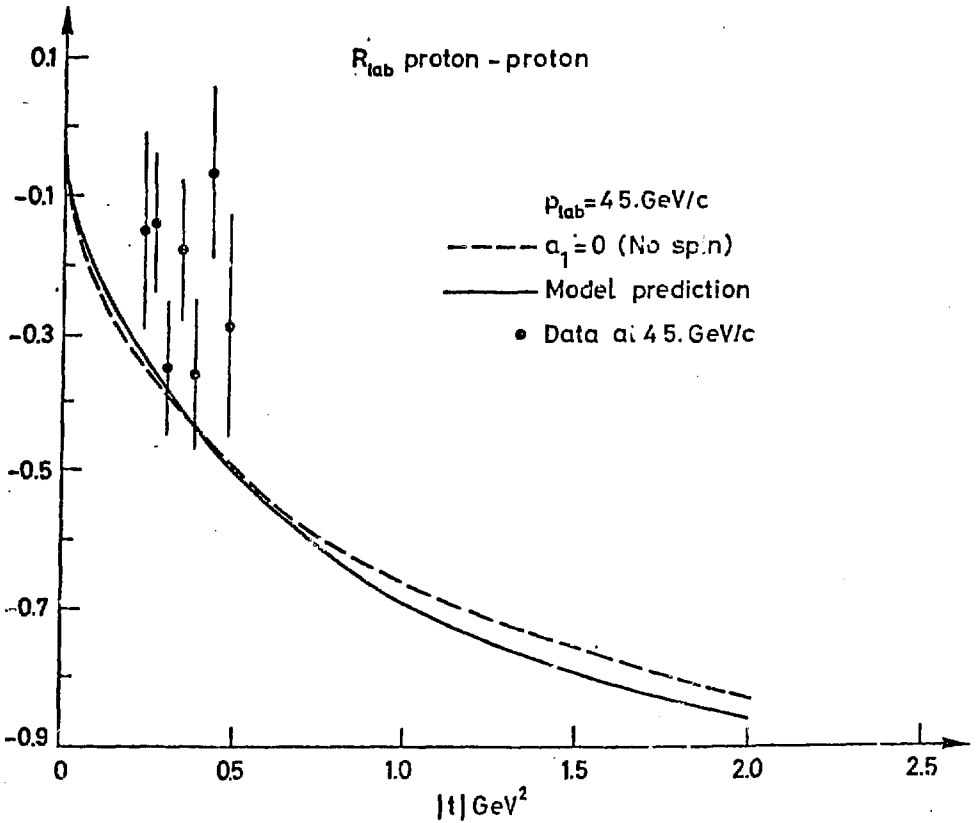
R_lab proton - proton
p_lab = 45. GeV/c
a_1 = 0 (No spin)
Model prediction
Data at 45. GeV/c
0.1
-0.1
-0.3
-0.5
-0.7
-0.9
0
0.5
1.0
1.5
2.0
2.5
|t| GeV²

Fig. 20

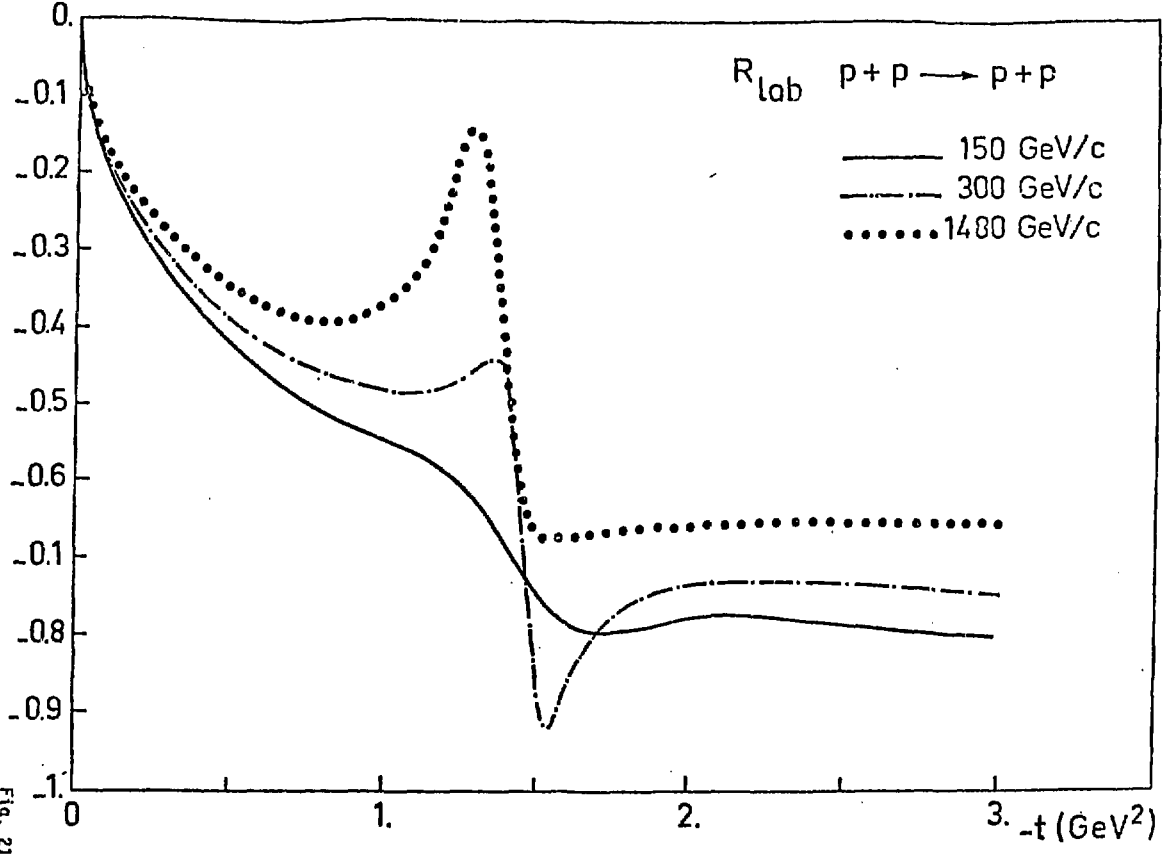
0.
-0.1
-0.2
-0.3
-0.4
-0.5
-0.6
-0.1
-0.8
-0.9
-1.
0
1.
2.
3.
-t (GeV²)
R lab p + p → p + p
150 GeV/c
300 GeV/c
1480 GeV/c

Fig. 21


3.
2.
1.
0
-1.
-t (GeV²)

Fig. 21

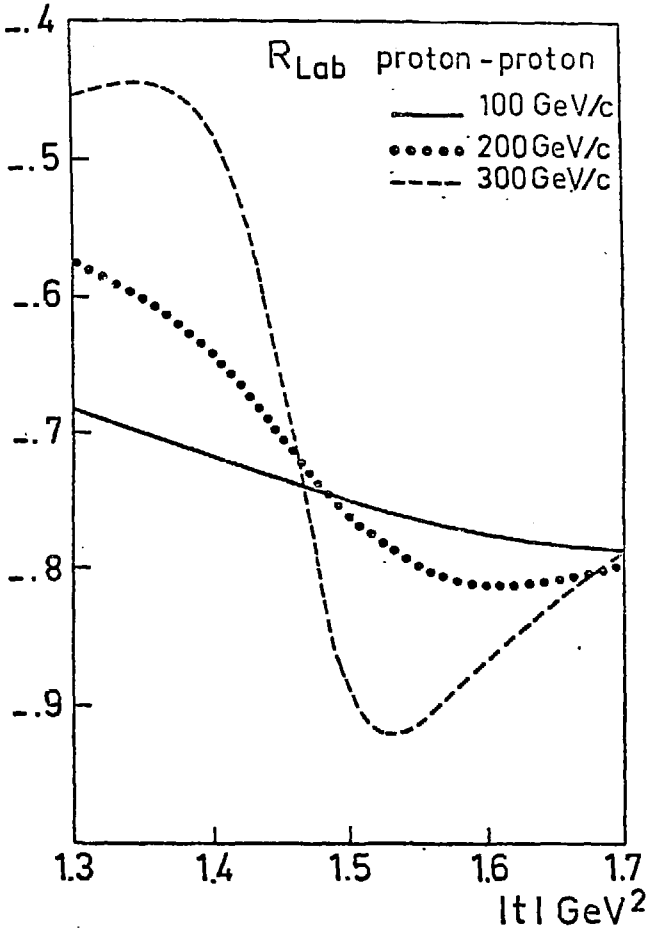
R_Lab proton-proton
100 GeV/c
200 GeV/c
300 GeV/c
-.4
-.5
-.6
-.7
-.8
-.9
1.3
1.4
1.5
1.6
1.7
|t| GeV²

Fig. 22